Journal of
Synchrotron
Radiation

ISSN 0909-0495

Received 10 March 2010
Accepted 5 May 2010

Diamond X-ray beam-position monitoring using signal readout at the synchrotron radiofrequency

J. Morse,[a]* B. Solar[b] and H. Graafsma[b]

[a]Instrumentation Services and Development Division, European Synchrotron Radiation Facility, Grenoble, France, and [b]Deutsches Elektronen Synchrotron, Hamburg, Germany.
E-mail: morse@esrf.fr

Single-crystal diamond is a material with great potential for the fabrication of X-ray photon beam-position monitors with submicrometre spatial resolution. Low X-ray absorption combined with radiation hardness and excellent thermal-mechanical properties make possible beam-transmissive diamond devices for monitoring synchrotron and free-electron laser X-ray beams. Tests were made using a white bending-magnet synchrotron X-ray beam at DESY to investigate the performance of a position-sensitive diamond device using radiofrequency readout electronics. The device uniformity and position response were measured in a 25 μm collimated X-ray beam with an I-Tech Libera 'Brilliance' system. This readout system was designed for position measurement and feedback control of the electron beam in the synchrotron storage ring, but, as shown here, it can also be used for accurate position readout of a quadrant-electrode single-crystal diamond sensor. The centre-of-gravity position of the F4 X-ray beam at the DORIS III synchrotron was measured with the diamond signal output digitally sampled at a rate of 130 Msample s^{-1} by the Brilliance system. Narrow-band filtering and digital averaging of the position signals resulted in a measured position noise below 50 nm (r.m.s.) for a 10 Hz bandwidth.

Keywords: diamond; beam-position monitor; radiofrequency; readout.

1. Introduction

In situ beam-position monitoring at the submicrometre level and with ∼kHz measurement bandwidth is increasingly important at synchrotron sources. Following the rapid development of nanoscience, X-ray synchrotron beams are now routinely focused down to submicrometre spots, with the target figure being 10 nm. Besides creating small focal spots, it is equally important to measure and, if possible, to stabilize the beam position on the sample with a resolution comparable with the beam size. This is especially challenging at synchrotron facilities owing to the long source–optics–sample distances involved which can reach up to 100 m or more. Small position and angular movements of the X-ray optics arise from thermal drifts, vibrational instabilities introduced by operating local equipment or *via* the floor itself. Angular movement of the beam upstream can translate into large position variations at the sample. At the same time data acquisition times are now often in the millisecond to second range, requiring that photon beam position monitor (pBPM) devices operate at comparable frequencies. pBPM devices with an accuracy level of typically ∼10% of the beam size are required either to correct for the effects of beam movements by post-processing corrections or, better still, as sensors for feed-back (or -forward) control systems to better stabilize the beam. It should be pointed out that feedback mechanisms generally involve moving relatively bulky optics, which limits the maximum frequency at which beams can be kept stable.

In the case of free-electron lasers, the distances between source and sample are even larger than at synchrotrons, in the range of several hundred metres, making the required stability for source and optics yet harder to reach. Furthermore, pulse-by-pulse position information is required since many experiments will be 'single shot' (Graafsma, 2009). Beside position monitors based on beam interactions with a gas, diamond is likely to prove the only material able to withstand the thermo-mechanical demands made by the European XFEL burst-mode operation, up to 2700 pulses in 600 μs, with 10^{12} photons $pulse^{-1}$. For the continuing miniaturization of the experiments at synchrotron and free-electron sources it is therefore crucial to develop *in situ* pBPMs with submicrometre sensitivity and kHz measurement rates.

Owing to its low atomic number ($Z = 6$), the absorption of 10 keV X-ray photons by diamond is about sevenfold less than for an equivalent thickness of silicon, and a 100 μm-thick diamond plate absorbs only 7.5% of the incident X-ray beam. This permits the permanent insertion into an X-ray beam of a mechanically robust diamond plate which can be operated as a solid-state position-sensitive 'ionization chamber'. These devices can be made extremely compact, occupying only a few

millimetres of space along the X-ray beam axis; they are insensitive to light of wavelengths above ~250 nm, and can be operated under ambient conditions at low bias voltages (~10–500 V dependent on the device thickness). Such practical mounting issues are of particular interest for X-ray nano-focusing requiring placement of a beam monitor between the final X-ray focusing optics and the sample where available space for the device may be less than a few centimetres. Diamond devices can also be safely operated below $\sim 10^{-3}$ mbar pressures, and the materials used in their fabrication are compatible with bake-out requirements of ultra-high-vacuum systems, *i.e.* $<10^{-8}$ mbar.

A further essential advantage of diamond is its radiation tolerance. For X-ray photon energies <250 keV, radiation-induced dislocation of the crystalline lattice of both diamond and silicon are energetically impossible. However, practical silicon devices may degrade in the X-ray beams owing to generation and trapping of charge in surface oxide layers used in their passivation, and surface currents associated with radiation-induced interface traps (Ma & Dressendorfer, 1989). A practical beam-monitoring device must operate in a stable manner over several months, preferably years, while the radiation dose rates in synchrotron undulator beams easily reach 10 kGy s^{-1} (Si). Position-sensing silicon diodes with linear resistive contacts have been thinned below 10 µm and successfully tested in synchrotron beams, but first devices showed sensitivity degradation with exposure (Fuchs *et al.*, 2008; Müller, 2010). Owing to its large bandgap, 5.45 eV, diamond shows no significant leakage current at room temperature, and indeed currents of $<10^{-14}$ A at >1 V μm^{-1} are observed experimentally on defect-free samples (Berdermann *et al.*, 2010). With suitable treatment the surface can have a chemically stable oxygen termination for which surface currents are also negligible with the sample under ambient conditions. Extensive measurements by the Cern RD42 collaboration (Kagan, 2005) with minimum ionizing particle beams at doses $>10^{15}$ cm^{-2} and with heavy ions by the NoRHDia collaboration (Pomorski *et al.*, 2007) have shown diamond to have a radiation hardness three to ten times greater than silicon, with reduction in charge collection efficiency but no increase in the negligible leakage current. Initial X-ray beam tests at the ESRF ID21 Microscopy Beamline of a diamond device with metal electrode contacts showed operational stability at a precision of <1% for an integrated X-ray beam dose of $>10^9$ Gy.

These advantages of diamond over silicon were realised several years ago by the synchrotron community, and X-ray pBPMs based on polycrystalline material were fabricated and tested (Bergonzo *et al.*, 2000; Schulze-Briese *et al.*, 2001). Polycrystalline chemical vapour deposition (CVD) diamond may be grown over large areas, for example on a silicon substrate, but diamond crystallites seed randomly on the surface with various orientations: these merge during the film growth process, forming grains of dimensions of ~10% of the film thickness. Charge trapping at the grain boundaries results in local deviations of an external electric field applied to the diamond, and this is observed as abrupt changes in the spatial electrical response, *i.e.* the measured charge collection efficiency (Tromson *et al.*, 2000). Such charge trapping, and possibly additional deep-level trapping from trace (<p.p.m.) levels of nitrogen incorporated in the diamond bulk from the growth process, result in complex signal time-lag effects and polarization of the material. To avoid these adverse effects, we employ ultra-high-purity single-crystal CVD diamond. This is grown homoepitaxially on single growth sector diamond seed crystals of [100] surface orientation. The growth layer is removed from the seed by laser cutting, and abrasively polished to a flat plate of thickness ~50 µm to 1 mm and size up to ~10 mm square. Further, non-abrasive polishing techniques such as ion-beam milling or plasma etching can give surfaces with local roughness as measured by atomic force microscopy (AFM) as low as 1 Å (r_a), and, importantly, with low damage of the subsurface crystal lattice (Friel *et al.*, 2009). This minimizes surface-related scatter and coherence loss of a transmitted X-ray beam, and the risk of subsurface charge trapping. 'Electronic grade' diamond material shows excellent electronic charge transport properties (Isberg *et al.*, 2002; Pernegger *et al.*, 2005; Pomorski *et al.*, 2005), and we have demonstrated complete collection of the electric charge generated by photoionization in an X-ray beam (Morse *et al.*, 2007). The spatial response of this material is uniform down to the submicrometre scale, and no significant beam-induced polarization effects are observed. As a result, devices can be made which, in principle, have position accuracy limited only by the precision of the readout electronics employed and/or statistics associated with the distribution of photons within the beam profile. For X-ray beam energies of ~10 keV, photoelectric and Compton interactions result in the generation of hot electrons which are thermalized within a few micrometres radius, and the subsequent diffusion spread of the electron–hole charge cloud that occurs during drift of this charge through a 100 µm plate thickness is ~10 µm. Signal currents can be measured with simple commercially available electrometers, and we have previously demonstrated that the centre of gravity position of an X-ray microbeam can be interpolated using quadrant electrode devices with a position noise of <15 nm r.m.s. (Morse *et al.*, 2007).

A further advantage of diamond beam monitors is that their electrical response can be extremely fast. Owing to the wide bandgap of diamond, strong electric drift fields can be applied without the generation of significant leakage currents. At a field of >2 V μm^{-1}, charge collection is completed within 1 ns for a 50 µm-thick single-crystal diamond plate. It is therefore possible to distinguish the time distribution of individual X-ray beam pulses at synchrotron sources, regardless of the machine bunch-fill operation modes. First experiments at the ESRF ID21 beamline using GHz bandwidth electronics demonstrated position sensitivity and leading-edge timing of the X-ray pulses with 20 ps r.m.s. jitter (Morse *et al.*, 2008). The position measurements we report on here have been made with a far better optimized signal-processing system, a modified I-Tech Libera Brilliance system (Instrumentation Technologies, Solkan, Slovenia; http://www.i-tech.si/), and confirm the potential of its narrow-band

RF signal-processing approach for fast and precise beam-position monitoring.

2. The diamond quadrant sensor

The single-crystal diamond plate samples used in our tests were supplied by Element Six (Ascot, UK; http://www.e6.com/). They are homoepitaxially grown by CVD using high-purity CH_4 and H_2 gases. Electron spin resonance analysis of a sample of this detector grade material showed no evidence of nitrogen impurity at a detection limit of <1 p.p.b. (Nebel, 2008), well within the manufacturer's specification of <5 p.p.b. single substitutional nitrogen. Two square diamond plates of side length 3.5 mm were abrasively 'scaife' polished, leaving a surface roughness of <1 nm (r_a) as measured by AFM, and final thicknesses of 382 and 389 µm. At the Ohio State University they were cleaned using hot oxidizing acids before further plasma cleaning and sputter deposition of ~100 nm-thick TiW metal electrodes. Lift-off mask lithography was used to define the contacts, giving a 12-electrode ringed-quadrant design on one side of each sample (Fig. 1*a*). The inner quadrant electrodes which together form a 2 mm-diameter circle are separated by a 50 µm isolation gap. The contacted diamonds were conductive epoxy glue bonded into ceramic carriers above a hole allowing passage of the X-ray beam, and the electrodes were connected by Al wedge wire bonding (Fig. 1*b*). For current voltage response (IV) tests at ESRF, the single electrode which covered the rear face of the diamond was biased, and the 'leakage' currents from the inner quadrant electrodes were measured. In air, these currents were ~30 pA at 500 V bias. Control tests with an empty ceramic carrier showed that these currents were primarily from leakage over the surface of the ceramic, and it was not possible to directly measure the smaller diamond leakage currents.

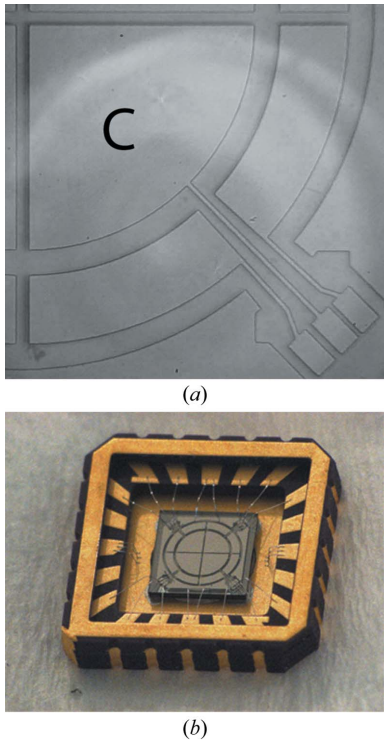

(*a*)

(*b*)

Figure 1
(*a*) Detail of a quarter of the diamond sensor TiW electrodes before wire bonding. The rear face of the detector has a single large-area contact pad, not visible in this image. (*b*) Diamond wire bonded in its ceramic carrier (3 mm hole under diamond not visible).

3. The Libera Brilliance system

The Brilliance instrument was developed as a readout system for electron beam position monitors (eBPMs). The Brilliance is designed for synchrotron storage rings, and with optimum input signal power it can attain position resolutions better than 50 p.p.m. with a 2 kHz measurement bandwidth. In its usual application the input signal power is determined by the beam properties (*e.g.* beam current, bunch pattern) and the sensitivity of the capacitive pick-ups used. The time development of the signals from the diamond pBPM we tested here are comparable with those generated by eBPM pick-up electrodes, but smaller in amplitude. Because of the wide diversity of photon beamline characteristics (*e.g.* flux, photon energies) the readout electronics of pBPMs in general require a wide amplitude dynamic and higher sensitivity than for the synchrotron eBPM application.

The Libera Brilliance readout system is effectively a four-channel narrow-passband RF voltmeter: it provides X and Y position information derived from four input voltage amplitudes signals V_A, V_B, V_C and V_D. After a first RF crossbar-switching system, each of its four parallel signal chains consist of a three-stage amplifier with a surface acoustic wave (SAW) bandpass filter, analog to digital converter (ADC), recombination and digital signal conditioning (DSC) block, bandpass filter and digital down converter (DDC) for accurate phase-independent calculation of the A,B,C,D signal amplitudes (Fig. 2). For these beamline measurements the SAW filters had a passband 5 MHz wide and tuned to the 500 MHz RF of the DORIS synchrotron. All components in the analog chain, including the 16-bit 130 Msample s^{-1} ADCs, are contained within the crossbar-switching system which periodically

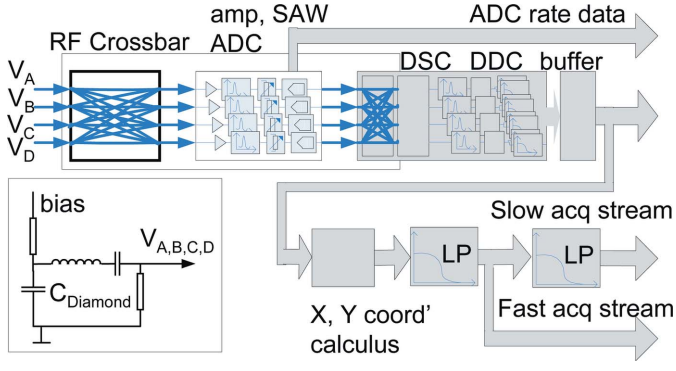

Figure 2
Block diagram of the internal architecture of the I-Tech Libera Brilliance beam-position instrument. The inset shows the passive elements used to couple input signals to the coaxial cables.

exchanges all four input signals over the four measurement channels; by this means the gain variations and drift of the individual channels are effectively removed or averaged over all channels. The switching rate is a compromise between an acceptable 'glitch' rate at each channel switching and the frequency response of the low-pass (LP) filter in the fast acquisition stream which periodically averages the switched signals. Glitches arise from the finite bandwidth transitions of the switched signals on the analog front and have crosstalk-like characteristics; with precise timing and synchronization of the switching these transitions are reproducible, which allows for their subsequent digital correction. For each signal/channel combination the DSC block identifies the channel amplitude and phase inequalities and makes the best possible corrections for these. The phase correction part of the DSC minimizes the effects of switching glitches in the DDC, while the amplitude part improves the fast acquisition stream LP filtering. The smooth slope of this LP filter guarantees low group delay necessary for implementing high-speed external signal feed-back control loops. The sampling frequency is chosen to ensure optimal operation of the ADCs and to be within the correct Nyquist zone for an under-sampled synchronously detuned sampling system; this reduces the effects of ADC and amplifier non-linearities. Several output paths provide position information in different formats, data rates and bandwidths. The most averaged data provide a slow acquisition stream with a user-defined bandwidth at a sample output rate up to 20 Hz. After a low slope and group delay LP filter, the fast acquisition data stream provides a 10 kHz sampling rate of 2 kHz signal bandwidth. This is optimized for beam stabilization feedback loops covering the spectrum of mechanical vibrations, and the data are available over a low-latency, 3 Gb s^{-1}, communication port. The fastest output stream provides unprocessed data at the full ADC sampling rate *via* a 2048 sample buffer.

For these first experiments with diamond pBPMs on the DORIS F4 beamline, simple modifications were made to a standard PETRA III eBPM Brilliance unit: a 5 dB higher-gain first amplifier stage was implemented, and an additional 6 dB input 'gain' achieved by removing two redundant 3 dB attenuators. These changes brought the Brilliance unit close to the optimum input gain requirements for our measurements. Note that the DORIS synchrotron operation mode consists of five positron bunches circulating with a revolution period of 0.96 µs, and the Brilliance system measured only the power from the diamond signal pulses that fell within its 5 MHz passband at 500 MHz.

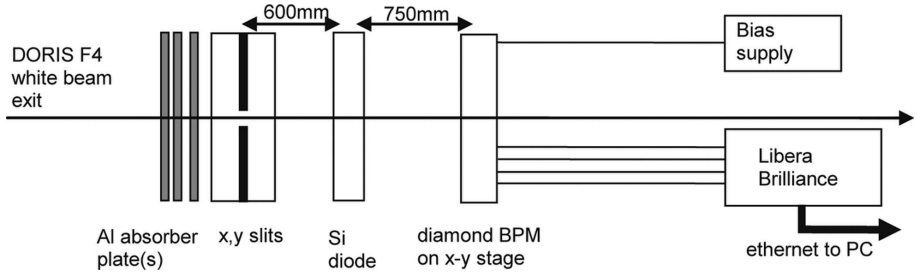

Figure 3
Arrangement of various components at the DESY F4 beamline hutch.

4. Experimental set-up at the DORIS synchrotron at DESY

For the DESY beamline tests presented here, the diamond quadrant detector in its ceramic carrier was mounted on a 30 mm-diameter printed circuit board (PCB) that enabled close assembly of some passive L, C and R components. These were bias resistors and small wire-coil inductances added in series with capacities $C_{\rm Diam} \simeq 0.5$ pF of the diamond quadrants, forming LC resonators at the 500 MHz RF and improving the signal coupling into the 50 Ω coaxial signal cables to the Brilliance. An additional coupling capacitor was used to block the DC signal path, simply as precaution to protect the Brilliance from the applied diamond voltage bias (see inset, Fig. 2). The PCB assembly was itself mounted in a metal box which provided electrical shielding and a simple means of mechanical mounting on the x,y translation stage. Fig. 3 shows the arrangement of the various components used for the beamline tests, with the diamond mounted downstream of a calibrated silicon photodiode and a pair of collimating slits. By a simple autocollimation technique we are certain that the beam intercepted the diamond at a perpendicular angle within an error of $<1^\circ$. Fig. 4 shows the energy distribution of the white beam flux from the DORIS III synchrotron bending magnet at the F4 beamline hutch, as calculated using the *XOP* program (Sanchez del Rio & Dejus, 2004) after collimation of the beam by the slits to 25 µm × 25 µm. The beam incident on the diamond sensor was filtered both by the 0.5 mm-thick silicon diode used to measure the beam intensity and by the various aluminium plates which were inserted to attenuate the beam intensity.

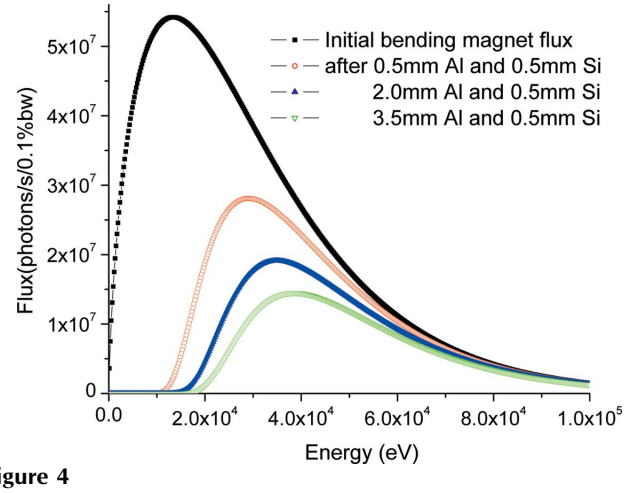

Figure 4
The *XOP*-calculated beam energy distribution at the DORIS F4 beamline. Flux values shown are for the beam after the 25 µm × 25 µm slits.

5. Measurement results

5.1. Area response uniformity

To locate its centre, the diamond sensor was first x,y spiral scanned in the beam while measuring the signal response of the four quadrants as a function of position using the A, B, C, D channels of the Brilliance system. Fig. 5(a) shows a coarse scan made of a large portion of the diamond and covering the B and C electrode quadrants. Here, the intensity scale corresponds to the sum over the A,B,C,D electrode signals that were read from the Brilliance after its digital averaging over a DC 10 Hz bandwidth. The signal amplitudes of the electrodes have been normalized in post-processing to account for the ∼20% variation seen in the maximum values which resulted from variations in RF cable insertion losses and gain differences between the individual channels. To remove the effect of the monotonic time-decay of the DORIS storage-ring current the data shown have also been corrected using the relative flux intensity measured by the silicon photodiode-electrometer. Fig. 5(b) shows the remaining few percent errors in channel normalization and response variation as the beam was scanned across the isolation region between the quadrant metal contacts. The response with the beam on the electrodes was flat within ∼1%. The leadout track from quadrant C to its wire bond pad also behaved as a photocurrent-collecting electrode, and this is clearly visible as the radial line at the bottom right in Fig. 5(a). The weak signal response from the outer-ring electrode adjacent to quadrant C may have resulted from a capacitive coupling crosstalk effect owing to poor grounding of this electrode.

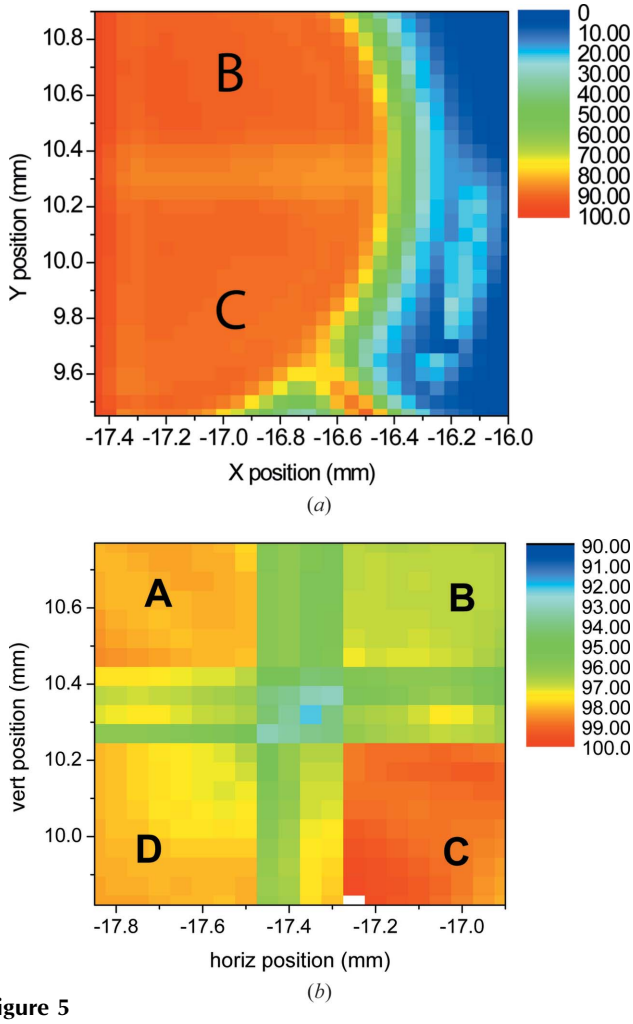

Figure 5
(a) Coarse spiral scan of the beam over the diamond at 50 µm steps. (b) Detail of the central region between quadrant electrodes with zoomed signal response scale. The physical isolation gap between the metal electrodes is 50 µm (bias 550 V, 0.5 mm Al attenuator).

5.2. Line scan data and position response

Fig. 6 shows a line scan across two quadrants at the approximate position indicated by the red arrow. Note that even when the beam is half way across electrode B (at horizontal position −16.8 mm) there is still a significant ∼15% signal response recorded on the neighbour electrode A. This is due to the capacitive coupling between these electrodes and their finite load impedance into the Brilliance signal cabling. Such crosstalk results in a proportional loss of useful signal power, *i.e.* it reduces the gradient of the signal slope between quadrants and thus the overall position sensitivity, but, assuming that it is a linear effect, it is not important otherwise. When the beam reaches position −16.5 mm, *i.e.* the outer edge of quadrant electrode B, the signal responses from both electrodes A and B fall to zero, confirming that there is no substantial beam halo contribution to the observed results.

Figs. 7(a) and 7(b) show horizontal line scans made across the geometric centre of the diamond. As the beam traverses the centre of the diamond, the position-sensitive 'crossover' response extends over ∼400 µm, far larger than the ∼25 µm width of the beam defined by the upstream slits. The signals do not fall to zero owing to the inter-electrode crosstalk effect. Over the bias values used, 138, 271 and 550 V, the signal measured by the Brilliance is seen to increase almost linearly by a factor of ∼2. The results contrast markedly with those measured with the same devices previously tested at the ESRF

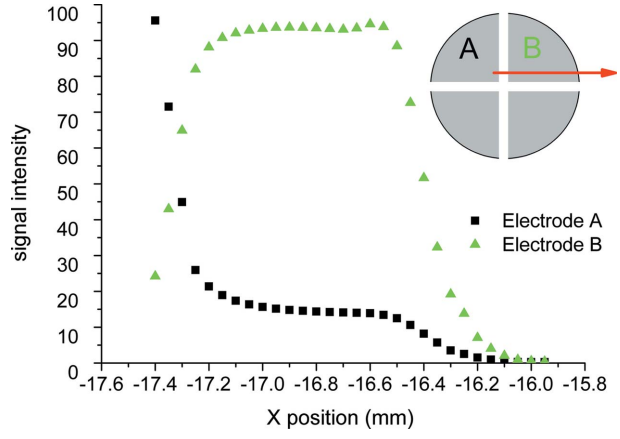

Figure 6
Line scan, diamond scanned horizontally across the beam (bias 550 V, 0.5 mm Al attenuator).

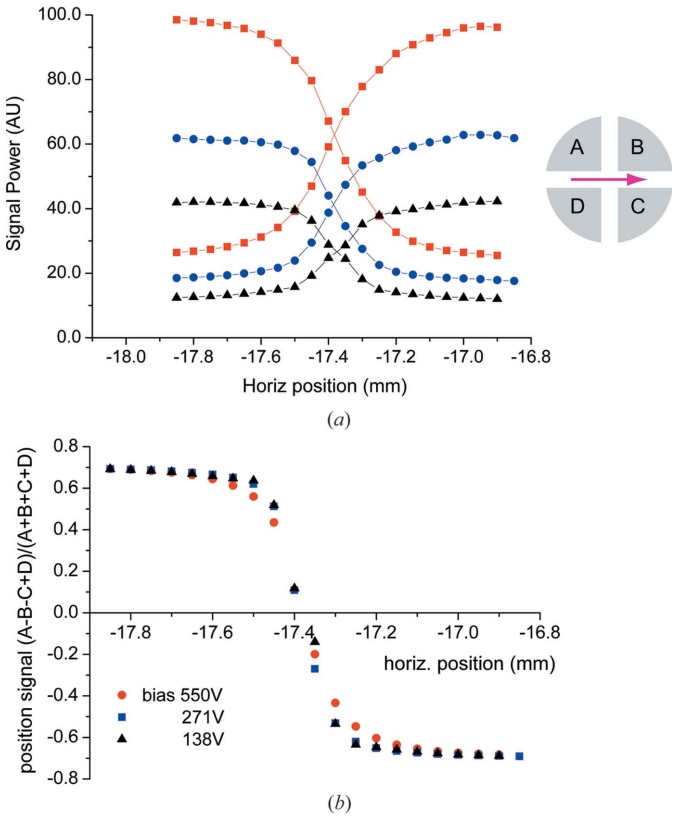

Figure 7
(*a*) Line scan showing diamond horizontal crossover signal responses ($A + D$), ($B + C$) at various bias values. (*b*) The same data after signal power normalization according to equation (1) (0.5 mm Al attenuator).

ID09B beamline, where the X-ray beam signal current response of the diamonds was seen to rise rapidly with applied bias voltage and plateau for values between 60 V and 500 V (the maximum applied). These differing results are interpreted as follows:

(i) With high-purity electronic-grade diamond, complete charge collection occurs for electric drift fields above $\sim$0.1 V μm^{-1} (Pomorski *et al.*, 2005). For the ID09B test, the signal currents induced by the X-ray beam were measured using current preamplifiers of 200 kHz bandwidth. As the diamond signal develops on a timescale of <10 ns, these amplifiers were insensitive to the precise drift velocities of the electron and hole charge carriers in the diamond.

(ii) In contrast, the Brilliance system used only measures the signal current power in a few MHz bandwidth centred at 500 MHz. As such, it measured just a fraction of the induction currents developed on the diamond electrodes by the charge moving in the diamond according to Ramo's theorem (Ramo, 1939); we therefore expect the response of the Brilliance to increase with increasing drift velocities of the charge carriers. These velocities increase with the applied electric field, and only saturate at $\sim$10 V μm^{-1} (Pomorski, 2009), to be compared with the fields of 0.3–1.4 V μm^{-1} used in the DESY tests. The crossover response also extends over a large distance when measured by the Brilliance, $\sim$400 μm as compared with $\sim$90 μm in the ID09B test (where the beam width itself was of similar size). This result is also explained by considering the spatial distribution of the induction field.

The horizontal position responsivity, normalized to remove the dependence on total signal power owing to variations in beam intensity *etc.*, is intuitively given by

$$(A - B - C + D)/(A + B + C + D), \qquad (1)$$

where A, B, C, D are the signal powers measured on each quadrant electrode. Fig. 7(*b*) shows that when so normalized, the position response width is almost independent of the applied bias, with a quasi-linear region that extends over $\sim$150 μm. At 550 V bias, a linear gradient fit in this region gave a position sensitivity of 0.39% μm^{-1}, expressed here as a percentage of the full signal swing observed as the X-ray beam is fully traversed left to right. With the bias reduced to 138 V, the position sensitivity, *i.e.* the gradient, increased by $\sim$34%, but the linear fits are subject to large errors, $\sim$17%.

5.3. Position sensitivity and response bandwidth

The position sensitivity of the system we define here as the minimum detectable beam-position movement that can be observed above noise in the measurements. To determine this, a series of time-trace measurements were made, *i.e.* recording the apparent position of the beam deduced from the measured A,B,C,D signal values while the position of the diamond remained fixed. The position-sensitivity 'calibration' figures obtained as described above were used to scale signal values onto the dimensional scale, and the position noise statistics of the time trace evaluated. An alternative, more direct, method of obtaining position sensitivity is to scan the diamond in the beam and measure the residual errors in plots of calculated position values *versus* real motor positions; however, this method inevitably introduces additional position noise arising from point-to-point variations in the motor-stepping intervals. Two-dimensional position maps made at 2 μm step intervals also showed features just visible above noise in the calculated positions which could easily be interpreted as small errors in motor positioning, so this method was not used. Fig. 8(*a*) shows a 0.4 s time trace of the vertical displacement of the beam, derived according to equation (1) and using the gradient calibration discussed above. These data were obtained with the beam initially centred between the four quadrants electrodes of the diamond sensor. The scatter of the individual data points corresponds to the 130 ksample s^{-1} sampling rate of the Brilliance 'data on demand' buffer. However, owing to a data acquisition software error, only two valid samples in every ten were recorded, and only these valid data points are depicted in Fig. 8(*a*) and used in the subsequent analysis. For both horizontal and vertical axes, Fig. 8(*b*) shows the 'position noise', *i.e.* its standard deviation, calculated over $\sim 10^3$ valid samples. These calculated standard deviations are presented after applying various low-pass-filter cut-off frequencies, F_c, below 100 Hz [refer to the OriginLab Corporation (http://www.originlab.com/) Origin 7.5 documentation for details of the low-pass filter and fast Fourier transform (FFT) algorithms used]. At these low frequencies

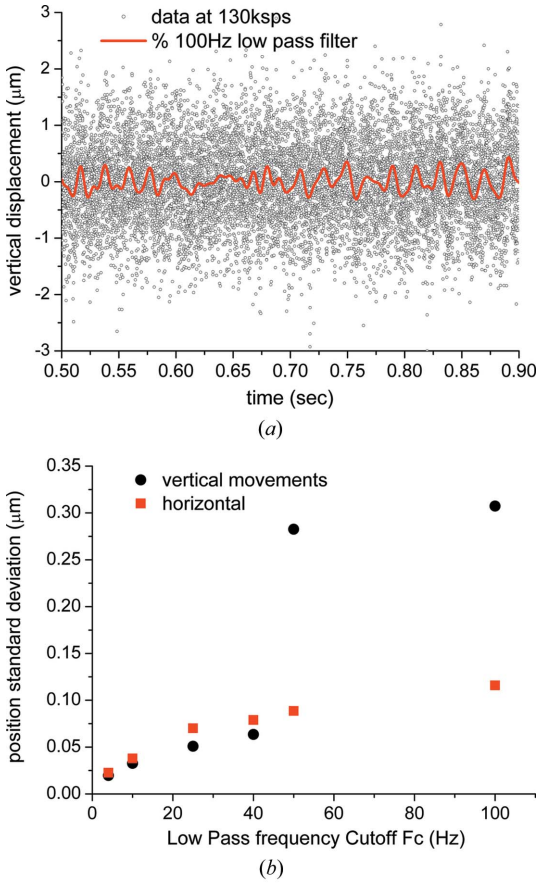

Figure 8
(*a*) Time trace showing scatter of vertical data positions calculated from Brilliance data buffer A,B,C,D values sampled at 130 ksample s^{-1}. (*b*) Standard deviations calculated for the same data for various low-pass bandwidth limits (0.5 mm Al attenuator, 550 V bias).

the use of just two out of every ten data points does not significantly affect the results. For a DC to 10 Hz bandwidth, the measured position noise is clearly below 50 nm for both vertical and horizontal traces. The position noise of the vertical trace only increases sharply to ∼300 nm when the bandwidth is increased to 50 Hz. Fig. 9(*a*) shows the same data in the frequency domain after applying a FFT; a noise peak at 49 Hz is clearly visible for the vertical axis with a smaller peak at ∼20 Hz for the horizontal axis. We believe these resonances resulted from vibration of the diamond mounting with respect to the beam. It is extremely unlikely that the vertical position peak at 49 Hz arises from line-frequency electronic interference as (i) this should affect equally both horizontal and vertical channels and (ii) the RF narrow bandwidth signal filtering of the Brilliance system completely rejects such low frequencies. The peak is, however, very likely a real vibration coupled from some extraneous system itself powered at 50 Hz AC line frequency. Fig. 9(*b*) shows data taken using the Brilliance at an earlier time but with a different mechanical mounting of the diamond. This shows, in this case at ∼62 Hz, a resonant mechanical response of the mounting arrangement to a deliberate external ground shock. It clearly demonstrates the capability of the diamond sensor system to track such disturbances.

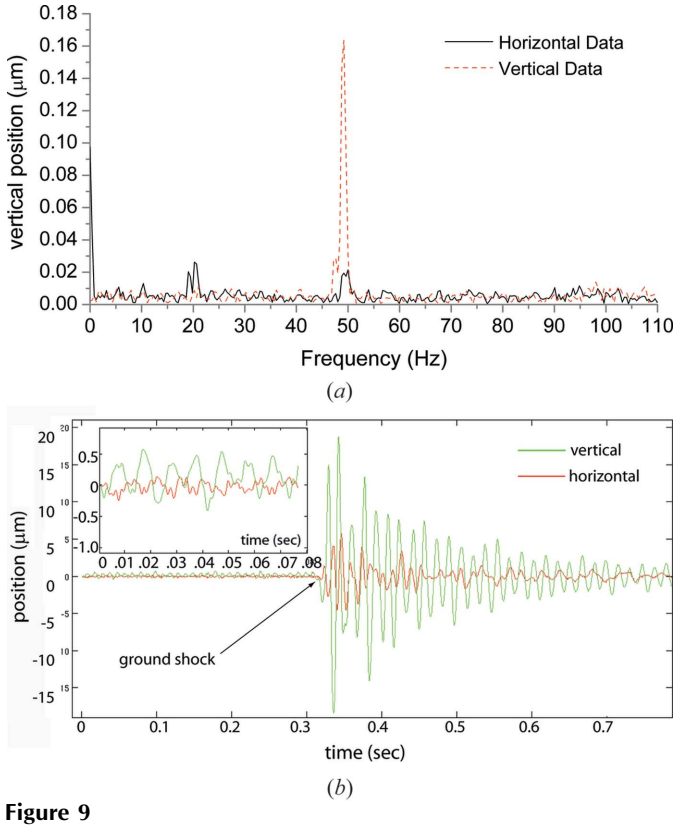

Figure 9
(*a*) FFTs of 3 s time trace data for both horizontal and vertical positions. (*b*) Time trace data from an earlier experiment measured with the same apparatus (the inset shows the position noise over a 1–1000 Hz bandwidth), and the response to an intentional ground shock.

6. Discussion

The 'position noise' results presented above are a convolution of the real movements of the X-ray beam with respect to the diamond pBPM and the electronic noise contribution of the Brilliance system itself. The position signal/noise ratio of the Brilliance improves with input signal power, reaching $\sim 4 \times 10^4$ at 10 ksample s^{-1} sampling rate under the condition of optimum input signal power within its passband. It is of interest to know how the signal/noise performance of the Brilliance varies with the beam flux incident on the diamond; this provides a direct benchmark of the performance of the system, and is far simpler than trying to quantify performance against the power-frequency distribution of the signal output by the diamond.

Using the *XOP*-determined flux–energy distribution shown in Fig. 4, the beam fluxes incident on the diamond were calculated. A Monte Carlo computer model was also developed to estimate the signal currents generated in the silicon photodiode and the diamond by photoelectric and Compton scattering interactions. Within a ∼10% error margin, the predicted current values for the silicon diode agreed with those actually measured using an electrometer, and this was the case for each of three beam attenuation conditions. The calculated fluxes incident on the diamond and the corresponding measured position noise values are given in Table 1. Note that for the diamond signal current estimates the

Table 1
Diamond position noise variation with beam intensity (bias 550 V).

Beam attenuator thickness (mm)	Flux on diamond (photons s^{-1})†	Horizontal position standard deviation (μm) (F_c = 40 Hz and *60 Hz*)	Vertical position standard deviation (μm) (F_c = 40 Hz and *60 Hz*)	Diamond beam transmission (%)†	Diamond current (μA)†
0.5 Al + 0.5 Si	1.09×10^{12}	0.079, *0.099*	0.064, *0.302*	97.11	3.54
2.0 Al + 0.5 Si	7.61×10^{11}	0.101, *0.123*	0.093, *0.222*	97.45	1.98
3.5 Al + 0.5 Si	5.86×10^{11}	0.128, *0.154*	0.131, *0.252*	97.50	1.49

† Values derived from computer models.

attenuation by the Ti(5%)–W(95%) electrodes, and the signal contribution from the contact near surface photoelectrons emitted into the diamond bulk, has been ignored.

It can be seen from Table 1 that the 0–40 Hz bandwidth position noise values decrease with increasing beam flux, which indicates that the electronic noise contribution of the Brilliance system is still a significant contribution to the total observed. Vertical and horizontal beam-position noises are similar when measured over a 0–40 Hz interval, but for 0–60 Hz the vertical noise degrades severely owing to the resonant frequency peak at 49 Hz [refer to Fig. 9(*a*)].

7. Conclusions

In our measurements we were not able to clearly separate the position noise contributions of the combined diamond pBPM and Brilliance measurement system from that of the real movements of the beam with respect to the diamond pBPM. Our use of a white beam of median energy ≥ 25 keV, for which Compton interactions in the diamond dominate the photoelectric effect, also makes a rigorous quantitative analysis difficult. Nevertheless, we have demonstrated that a quadrant diamond sensor can be operated with RF readout and give a 'worst case' total measurement precision that is submicrometre over a bandwidth exceeding 100 Hz.

Better understanding of the spatial extent of the position response crossover region requires a detailed modelling of the dynamics of the charge-carrier drift motion in the diamond and the frequency response of the Brilliance to the signal currents generated; this work has now begun. In addition, quantitative comparisons of the relative performance of narrow-band RF readout as compared with the conventional electrometer approach must be made, and ideally these must be carried out using a monochromatic X-ray beam with two identical devices to permit direct subtraction of the beam vibration contributions to the measured total position noise.

Practical issues also need to be considered in real beamline applications: the narrow-band RF approach uses low-impedance circuitry, and outside of its signal-pass band it has near complete rejection of extraneous noise-error sources. In contrast, leakage current noise and drift, line frequency and other sources of electronic interference all make difficult accurate position measurements with high input-impedance electrometer systems. Leakage current is usually insignificant in diamond, but may be problematic for poor-quality samples with localized bulk defects, and the insulating surface of diamond might also degrade by contamination over time if a device is not operated in a clean environment. The Brilliance system may also be considered for use with voltage-biased thin silicon devices for which large temperature-dependent leakage currents are certain. Long-term aging and radiation stability testing of devices in real beamline applications have yet to be carried out, and the choice of readout technique employed in the measurements may be a determinant factor in the quality of the results obtained.

We are particularly grateful to Professor Harris Kagan, Ohio State University, for the contact processing and mounting of the diamond samples used in these tests. Dr James Grant, University of Glasgow, produced the lithographic mask for these devices. The single-crystal 'electronic grade' CVD diamond substrates used in these tests were supplied by Element Six (Ascot, UK) and polished at Element Six (Cuijk, The Netherlands). U. Trunk and G. Potdevin of the DESY Laboratory are acknowledged for their support during the various measurement campaigns at the DESY F4 beamlines; Liam Gannon, University of Bath, for his important contribution to processing the data. This work was carried out as part of the DIMOX collaboration between DESY and ESRF for the development of diamond beam-monitoring systems.

References

Berdermann, E., Pomorski, M., de Boer, W., Ciobanu, M., Dunst, S., Grah, C., Kiš, M., Koenig, W., Lange, W., Lohmann, W., Lovrinčić, R., Moritz, P., Morse, J., Mueller, S., Pucci, A., Schreck, M., Rahman, S. & Träger, M. (2010). *Diamond Relat. Mater.* **19**, 358–367.

Bergonzo, P., Brambilla, A., Tromson, D., Mer, C., Hordequin, C., Guizard, B., Foulon, F., Solé, V. A. & Gauthier, C. (2000). *Diamond Relat. Mater.* **9**, 960–964.

Friel, I., Clewes, S., Dhillon, H., Perkins, N., Twitchen, D. & Scarsbrook, G. (2009). *Diamond Relat. Mater.* **18**, 808–815.

Fuchs, M., Holldack, K., Bullough, M., Walsh, S., Wilburn, C., Erko, A., Schäfers, F. & Mueller, U. (2008). *Rev. Sci. Instrum.* **79**, 063103.

Graafsma, H. (2009). *J. Instrum.* **4**, P12011.

Isberg, J., Hammersberg, J., Johansson, E., Wikström, T., Twitchen, D., Whitehead, A., Coe, S. & Scarsbrook, G. (2002). *Science*, **297**, 1670–1672.

Kagan, H. (2005). *Nucl. Instrum. Methods Phys. Res. A*, **546**, 222–227.

Ma, T. P. & Dressendorfer, P. V. (1989). *Ionizing Radiation Effects in MOS Devices and Circuits.* New York: Wiley.

Morse, J., Salomé, M., Berdermann, E., Pomorski, M., Cunningham, W. & Grant, J. (2007). *Diamond Relat. Mater.* **16**, 1049–1052.

Morse, J., Salomé, M., Berdermann, E., Pomorski, M., Grant, J., O'Shea, V. & Ilinski, P. (2008). *Mater. Res. Soc. Symp. Proc.* 1039-P06-02.

Müller, U. (2010). Private communication.

Nebel, Ch. (2008). Private communication.

Pernegger, H., Roe, S., Weilhammer, P., Eremin, V., Frais-Kölbl, H., Griesmayer, E., Kagan, H., Schnetzer, S., Stone, R., Trischuk, W., Twitchen, D. & Whitehead, A. (2005). *J. Appl. Phys.* **97**, 073704.

Pomorski, M. (2009). PhD thesis, University of Frankfurt, Germany.

Pomorski, M., Berdermann, E., Ciobanu, M., Martemyianov, A., Moritz, P., Rebisz, M. & Marczewska, B. (2005). *Phys. Status Solidi A*, **202**, 2199–2205.
Pomorski, M., Berdermann, E., de Boer, W., Furgeri, A., Sander, C. & Morse, J. (2007). *Diamond Relat. Mater.* **16**, 1066–1069.
Ramo, S. (1939). *Proc. IRE*, **27**, 584–585.
Sanchez del Rio, M. & Dejus, R. J. (2004). *Proc. SPIE*, **5536**, 171–174.
Schulze-Briese, C., Ketterer, B., Pradervand, C., Brönnimann, C., David, C., Horisberger, R., Puig-Molina, A. & Graafsma, H. (2001). *Nucl. Instrum. Methods Phys. Res. A*, **467–468**, 230–234.
Tromson, D., Brambilla, A., Foulon, F., Mer, C., Guizard, B., Barrett, R. & Bergonzo, P. (2000). *Diamond Relat. Mater.* **9**, 1850–1855.